Denitrification by large NAT particles: the impact of reduced settling velocities and hints on particle characteristics

W. Woiwode[1]**, J.-U. Grooß**[2]**, H. Oelhaf**[1]**, S. Molleker**[3]**, S. Borrmann**[3]**, A. Ebersoldt**[4]**,
W. Frey**[3,*]**, T. Gulde**[1]**, S. Khaykin**[5,**]**, G. Maucher**[1]**, C. Piesch**[1]**, and J. Orphal**[1]

[1]Institute for Meteorology and Climate Research, Karlsruhe Institute of Technology, Karlsruhe, Germany
[2]Institute of Energy and Climate Research – Stratosphere (IEK-7), Forschungszentrum Jülich, Jülich, Germany
[3]Max Planck Institute for Chemistry, Particle Chemistry Department, Mainz, Germany
[4]Institute for Data Processing and Electronics, Karlsruhe Institute of Technology, Karlsruhe, Germany
[5]Central Aerological Observatory, Dolgoprudny, Moscow region, Russia
[*]now at: School of Earth Sciences, The University of Melbourne, Melbourne, Victoria, Australia
[**]now at: LATMOS, CNRS-INSU, Université de Versailles St. Quentin, Guyancourt, France

Correspondence to: W. Woiwode (wolfgang.woiwode@kit.edu)

Abstract

Vertical redistribution of HNO_3 through condensation, sedimentation and evaporation of large HNO_3-containing particles inside polar stratospheric clouds (PSCs) plays an important role in the chemistry of the Arctic winter stratosphere. During the RECONCILE campaign, apparent very large NAT (nitric acid trihydrate) particles were observed in situ by the particle probe FSSP-100 inside PSCs. The observations can hardly be explained assuming particles with compact morphology and spherical shape due to limited growing time at temperatures below the existence temperature of NAT (T_{NAT}). Utilizing state-of-the-art simulations by the CLaMS and observations by the airborne Fourier transform infrared spectrometer MIPAS-STR we present a case study on the impact of reduced settling velocities of NAT particles on vertical HNO_3 redistribution. The results of our study show that reduced settling velocities of NAT particles significantly modify the simulated vertical HNO_3 redistribution and settling velocity is an important parameter in simulations. Our comparisons of simulated and observed HNO_3 redistribution show good agreement especially when moderately reduced settling velocities are considered. While simulated denitrification also depends critically on other parameters of the simulation not investigated here, we speculate that the large apparent NAT particles observed in situ on 25 January 2010 might have been compact aspheric (e.g. elongated) particles. Such particles could grow to largest maximum sizes in a short time while having only moderately reduced settling velocities that were best compatible with our results.

1 Introduction

Irreversible vertical redistribution of HNO_3 through denitrification plays an important role in Arctic ozone depletion chemistry (Solomon, 1999 and references therein). The freezing out of HNO_3-containing particles at altitudes above ca. $18\,km$ followed by sedimentation delays the deactivation of ozone-destroying substances by limiting NO_x (reactive nitrogen oxide radicals) availability from HNO_3 photolysis. Furthermore, the formation of liquid and solid PSC particles and the reactive surface capable of chlorine activation depend on HNO_3 availability in the

gas phase (Grooß et al., 2005 and references therein). Particles capable of denitrification are assumed to be composed of NAT, ice-coated NAT and potentially also further metastable phases composed of HNO_3 and H_2O, with NAD (nitric acid dihydrate) being one of the most likely candidates (Hanson and Mauersberger, 1988; Worsnop et al., 1993; Peter and Grooß, 2012 and references therein). Potential higher hydrates of HNO_3 are also reported in the literature (Marti and Mauersberger, 1994; Tabazadeh and Toon, 1996), while experimental evidence is sparse. Measurements of large HNO_3-containing particles with significant potential to denitrify the lower stratosphere were reported by Fahey et al. (2001).

In situ observations by the FSSP-100 (Forward Scattering Spectrometer Probe 100) during the Arctic RECONCILE (Reconciliation of essential process parameters for an enhanced predictability of Arctic stratospheric ozone loss and its climate interactions) field campaign in early 2010 aboard the high altitude research aircraft M55 Geophysica indicate potential NAT particles with unexpected large sizes and high number densities (von Hobe et al., 2013; Molleker et al., 2014). Such large NAT particles can hardly be explained with current theory of particle growth and sedimentation assuming approximately spherical shape, compact morphology and particle mass density described in literature, as will be shown in this work for the flight on 25 January 2010.

The properties of μm-size ice particles in the atmosphere are well known (Libbrecht, 2005 and references therein). Depending on the crystallization conditions, plates, needles and more complex crystals are found, with many of the particles found being considerably aspheric. In contrast, detailed knowledge on the shape and morphology of stratospheric HNO_3-containing particles causing denitrification is lacking. Films of HNO_3-containing particles near the composition of NAT were characterised by Keyser et al. (1993) under laboratory conditions. The authors report granular μm-sized particles forming aggregates.

Grothe et al. (2006) analysed the shapes of μm-sized NAT particles under laboratory conditions while investigating the crystallisation kinetics in the presence and absence of ice domains. In the absence of ice domains they obtained plates with diameters in the order of microns, whereas needles grew in the presence of ice. Wagner et al. (2005) reported NAD particles obtained in the cloud chamber AIDA (Aerosol Interactions and Dynamics in the Atmosphere),

and their spectroscopic measurements are best explained by assuming significantly oblate particles. Hence, large HNO_3-containing particles in the stratosphere causing denitrification might be partially composed of aspheric NAD particles, and such particles might act as templates for large NAT particles resulting from transformation of metastable NAD into NAT.

In this work we use measurements of gas-phase HNO_3 from the airborne Fourier transform infrared spectrometer MIPAS-STR (Michelson Interferometer for Passive Atmospheric Sounding-STRatospheric aircraft) (Piesch et al., 1996; Woiwode et al., 2012 and references therein) deployed aboard the high altitude aircraft Geophysica to study denitrification inside the Arctic polar vortex at the end of January 2010. The MIPAS-STR measurements resolve structures resulting from vertical HNO_3 redistribution with vertical extensions in the order of 1 km and horizontal extensions of several tens of kilometres along flight track and provide information on cloud coverage and temperature.

We use simulations from the CLaMS (Chemical Langrangian Model of the Stratosphere) (Grooß et al., 2005) to analyse the formation conditions of potential NAT particles sampled in situ by the FSSP-100 under the conditions of the Geophysica flight on 25 January 2010. Furthermore, we test the sensitivity of vertical HNO_3 redistribution on reduced sedimentation velocities of simulated NAT particles and compare vertical distributions of simulated gas-phase HNO_3 with the MIPAS-STR observations. Finally, we discuss potential properties of particles involved in denitrification in the context of measured and simulated vertical redistribution of HNO_3 and the in situ particle observations.

The combination of literature review (above) and measurements presented in this study lead to the following assumptions considered in this work: (i) stratospheric HNO_3-containing particles might be approximately spherical, but consist of loosely packed aggregates of smaller subunits and therefore have a reduced net particle mass density compared to compact spherical particles and (ii) these particles might be compact but significantly aspheric (i.e. needle- or disk-shaped). Both assumptions would allow growth of particles with larger maximum sizes (i.e. diameter or length) compared to compact spherical particles, which are often assumed in simulations for simplification. And in both cases, characteristically reduced settling velocities were expected, altering the vertical redistribution of HNO_3.

4

This study complements a previous study by Woiwode (2013) and takes into account the finalised CLaMS setup for the Arctic winter 2009/10, considering the new saturation-dependent parameterisation of heterogeneous NAT nucleation rates introduced by Grooß et al. (2014) and based on the results of Hoyle et al. (2013).

2 Campaign, observations and model

The RECONCILE field campaign was carried out from January until March 2010 and was based in Kiruna, Sweden (von Hobe et al., 2013). Flights of the high altitude aircraft M55 Geophysica allowed probing of the polar vortex with in situ and remote sensing instruments, including the particle probe FSSP-100 and MIPAS-STR. As discussed by Dörnbrack et al. (2012), a strong and cold vortex was formed in the middle of December 2009. The subsequent mid-winter period was exceptionally cold, allowing the existence of synoptic scale PSCs until the end of January 2010 and resulting in strong denitrification (Khosrawi et al., 2011). Space-borne lidar observations indicated PSCs composed of mixtures of NAT and STS (Supercooled Ternary Solutions, composed of H_2O, HNO_3 and H_2SO_4) inside the Arctic vortex at the end of January 2010 (Pitts et al., 2011).

The measurements from the FSSP-100 (de Reus et al., 2009) are designated for studying the abundances and sizes of µm-sized particles. The FSSP-100 is capable of detecting particles with sizes in the range of about $1.05\,\mu m$ to $37.5\,\mu m$ based on single forward scattering of laser light. The measurements are usually evaluated considering the Mie Theory, assuming approximately spherical particles. Advanced methods (not applied here) allow for the determination of accurate size distributions of aspheric particles, taking into account a priori knowledge on particle shape (Borrmann et al., 2000). In situ PSC observations during the RECONCILE period and in December 2011 are discussed by Molleker et al. (2014). For aspheric particles a broadening of the FSSP size distribution would be expected and the particle volume would be stronger affected by the oversized part. While for particles with aspect ratios of 2 already significant changes in the size distribution have to be taken into account (Borrmann et al., 2000), largest changes are

expected for particles with considerably higher aspect ratios. This aspect is however not further exploited here.

The MIPAS-STR limb- and upward-viewing measurements allow for the reconstruction of vertical profiles and cross-sections of temperature and trace gas distributions along flight track and provide information on cloud coverage. Details on the MIPAS-STR sampling and data processing are discussed by Woiwode et al. (2012). Forward calculations and inversion of the MIPAS-STR measurements were carried out using the forward model KOPRA (Karlsruhe Optimised and Precise Radiation transfer Algorithm; Stiller et al., 2002) and the inversion module KOPRAFIT (Höpfner et al., 2001), using the Tikhononv Phillips regularization approach (Tikhonov, 1963; Phillips, 1962). Retrievals were carried out utilizing a regular vertical $0.5\,\mathrm{km}$ grid in the considered vertical range (grid-spacing increases at higher altitudes). Observations with tangent points lower than $12\,\mathrm{km}$ were omitted to avoid tradeoffs in regularisation. Vertical resolutions given in this context were estimated according to Purser and Huang (1993). Temperature was retrieved utilizing the CO_2 signatures in the microwindows from 810.1 to $813.1\,\mathrm{cm}^{-1}$ and 955.6 to $958.5\,\mathrm{cm}^{-1}$. Subsequently HNO_3 was retrieved using the signatures in the microwindow from 866.0 to $870.0\,\mathrm{cm}^{-1}$. Retrieval parameters were the target parameter (temperature or volume mixing ratio), wavenumber-independent background continuum, spectral shift and O_3 as additional parameter in the temperature retrieval. Total combined 1σ-uncertainties were estimated considering uncertainties due to spectral noise, radiometric calibration, spectroscopic line data, line-of-sight knowledge, the adopted CO_2 profile (temperature retrieval) and retrieved temperature (HNO_3 retrieval). Details on the MIPAS-STR retrieval and its validation are discussed by Woiwode et al. (2012).

No cloud filtering according to Spang et al. (2004) omitting stratospheric spectra with low cloud index values was performed. Practically all stratospheric limb measurements associated to the flight on 25 January 2010 showed cloud index values below 4, indicating that the flight was carried out inside PSC clouds. The highest limb views exhibited minimum cloud index values as low as 1.6 as a consequence of continuum-absorption by PSC particles. The spectra however showed clear trace gas emission signatures suitable for retrievals of atmospheric parameters.

6

Moderate continuum-like contributions from aerosols are typical for mid-infrared limb observations of the upper troposphere/lower stratosphere (UTLS) region and are considered in the MIPAS-STR data processing by the reconstruction of wave number-independent background continuum. As for the flight on 25 January 2010 spectra with rather low cloud index values were included, wave number-independent background continuum was inverted logarithmically, resulting in low residuals between the observed and simulated spectra close to the noise level.

This approach meets the high dynamical range in the continuum background between spectra associated to different vertical viewing angles, especially at the lower boundaries of PSCs, where the continuum background can decrease sharply. Pressure-broadened tropospheric H_2O and CO_2 signatures as described by Höpfner et al. (2004) indicating scattering of tropospheric radiation by PSC particles into the MIPAS-STR field-of-view at high limb views were not identified. However, the H_2O retrieval was not exploited for this flight considering the weak intensity of the utilized H_2O signature under the conditions of this flight and the resulting high uncertainties and low vertical resolution of the retrieval results. Furthermore it was not clear whether potential weak contributions of scattered tropospheric radiation not obviously identified in the spectra might significantly alter the weak H_2O signature observed at higher viewing angles.

The CLaMS provides full three-dimensional simulation of both stratospheric chemistry and particle sedimentation based on the Lagrangian concept. Details on the simulation of particle nucleation, growth and sedimentation are given by Grooß et al. (2014) (references therein). The authors successfully applied CLaMS for simulating denitrification in the Arctic winter 2009/10, utilizing a new saturation-dependent parameterisation for heterogeneous nucleation rates of NAT (see Hoyle et al., 2013). Growth and sedimentation of large NAT particles at temperatures below T_{NAT} are simulated according to Carslaw et al. (2002). Spherical NAT particles with a particle mass density of $1.62\,\mathrm{g\,cm^{-3}}$ (compare Drdla et al., 1993) are assumed in the standard scenario. Horizontal advection is simulated on isentropic levels based on background wind fields provided by ECMWF (European Centre for Medium-Range Weather Forecasts) ERA-Interim reanalyses. Vertical sedimentation of NAT particles is computed considering gravitational settling and the viscosity of air. The sedimentation velocities are calculated according

to the Stokes equation (i.e. Pruppacher and Klett, 1997) and under consideration of the Cunningham correction for slip flow for spherical particles (i.e. Müller and Peter, 1992). The horizontal resolution of the considered CLaMS simulations is about 70 km and the vertical resolution is about 0.7 km.

3   In situ particle measurements and backward trajectories

During RECONCILE flights probing potentially NAT-containing PSCs the FSSP-100 instrument detected large particles with diameters of more than 20 μm at temperatures above the frost point (von Hobe et al., 2013; Molleker et al., 2014). Figure 1 shows an exemplary FSSP-100 size distribution associated to the vortex flight on 25 January 2010. Two main modes peaking at diameters of about 5.5 μm and 14 μm with very high number densities of about 0.004 cm^{-3} and 0.007 cm^{-3} can be identified, respectively. Particles with extremely large diameters higher than 20 μm are found. The maximum number density of the second mode is about a factor of 5 higher than the maximum of the large NAT mode reported by Fahey et al. (2001) peaking at 14.5 μm. In the shown representation indicating differential number densities the large NAT mode discussed by Fahey et al. (2001) peaks at about 0.0014 cm^{-3} (compare Molleker et al., 2014). Assuming spherical particles, the HNO$_3$ content of the complete size distribution is estimated to be equivalent to about 11.5 ppbv of gas phase HNO$_3$ considering an ambient temperature of 195 K and a pressure of 60 mBar. Thereby, 11 ppbv would correspond to the size bins higher than 9.5 μm.

Figure 1 shows also the associated size distribution corresponding to the CLaMS standard scenario (see Sect. 5) assuming compact spherical particles. The particle mode situated between about 5 and 12 μm and causing the simulated denitrification is by a factor of 1.5 to 13 lower compared to the observed number densities in this size range. The largest particles observed with sizes above 12 μm are not reproduced by the simulation. One possible (partial) explanation for the observed discrepancy might be that NAT particles have larger optically apparent sizes (diameter or length) compared to compact spherical particles due to non-compact morphology and/or aspheric shapes. The small particle mode below 2 μm corresponds to simu-

8

lated STS droplets. The high number density mode of small NAT particles described by Grooß et al. (2005) was not considered in the discussed simulations. Also shown in Figure 1 is the corresponding size distribution obtained when a negative temperature bias of 1 K is considered in the simulation. While the shape of the NAT mode is modified, this setup also fails to reproduce the particles larger than $12\,\mu m$ indicated by the observation.

For 8 of the simulated particles with diameters between 6 to $12\,\mu m$ and corresponding to the standard scenario backward trajectories were reconstructed and continued by airmass trajectories prior to the nucleation event. The obtained trajectories are presented in Figure 2 together with the flight track of the Geophysica on 25 January 2010. The extracted trajectories beginning at 07:00 UTC show the following characteristics: (i) the trajectories remain compact during the entire interval of about 4.5 days considered, indicating the absence of significant shear in the flow of the overlaying airmasses passed by the individual particles at different times as a consequence of different settling velocities. (ii) All trajectories reach T_{NAT} (typically between 194 K to 198 K, depending on the actual partial pressures of H_2O and HNO_3) around the north-east coast of Greenland about 2 days prior to the FSSP-100 measurements, resulting in growth of the simulated compact spherical particles to maximum diameters of less than $12\,\mu m$ in the CLaMS domain. (iii) Going further back in time the temperatures of the associated air parcels further increase. Temperatures of 210 K (red triangles) are reached about 2.8 days prior to the in situ particle observations. (iv) Temperature profiles between $80°$ and $90°$ N perpendicular to the locations where the trajectories reach about 210 K (blue asterisks connected by line) show all temperatures well above T_{NAT} in the vertical range considered (inset in Fig. 2). Considering that the ambient regions were also characterised by temperatures above T_{NAT} and the compactness of the trajectories for particles with diameters between 6 to $12\,\mu m$ it appears unlikely that larger particles have entered the locations of the discussed particle observations along very different trajectories.

So in summary, for the flight on 25 January 2010 the CLaMS simulation results in growth of compact spherical particles with maximum diameters smaller than $12\,\mu m$ as a consequence of limited growing time. In contrast, the FSSP-100 observations shown in Figure 1 indicate potential NAT particles with maximum sizes larger than $20\,\mu m$.

4 MIPAS-STR measurements of PSC coverage and gas-phase HNO_3

For the flight on 25 January 2010 (start 05:50 UTC and landing 9:19 UTC in Kiruna, Sweden), the flight track of the Geophysica and the horizontal distribution of the tangent points associated to the MIPAS-STR observations are shown in Figure 3. Practically all MIPAS-STR observations were located inside the polar vortex. The tangent points of the MIPAS-STR observations subsequently covered the regions labelled with A, B and C. During the turn around 07:30 UTC further scans named B_1, B_2 and B_3 were performed. Between the scans B_3 and C sampling was interrupted as the instrument was pointing towards the rising sun.

In Figure 4 the retrieved vertical distribution of wave number-independent continuum absorption for the 810.1 to 813.1 cm^{-1} microwindow associated to the temperature retrieval is shown for the flight on 25 January 2010. The interval of the FSSP-100 measurements (Fig. 1) and the starting positions of the particle backward trajectories (Fig. 2) correspond to section B. Enhanced continuum absorption qualitatively indicates the presence of cloud and aerosol particles. Along almost the entire flight track, significantly increased continuum absorption indicates the presence of PSC particles around flight altitude and above. A pronounced maximum is found in the section between 06:15 to 07:10 UTC, with a sharp contrast to low continuum absorption indicating the absence of continuum absorbers below about 17.5 to 18.0 km. In the last part of the flight between 08:15 and 08:45 UTC, enhanced continuum absorption is found at altitudes higher than 17 km, with local minima around 18.0 to 18.5 km, suggesting different PSC layers. Also shown is the level where the retrieved temperatures from MIPAS-STR are equal to the existence temperature of NAT (at higher altitudes the retrieved temperatures are below T_{NAT}). T_{NAT} was calculated considering the MIPAS-STR retrieval results of HNO_3 (typical vertical resolution about 1 km) and temperature (typical vertical resolution about 2 km) in combination with a smoothed vertical profile of H_2O constructed from the in situ observations of FLASH-A (Khaykin et al., 2013) during the ascent and descent phase of the Geophysica associated to the discussed flight (i.e. H_2O volume mixing ratios of 4.2 ppmv below 17.5 km and values within 4.2 to 5 ppmv at higher altitudes). Thermodynamic parameters for the calculation of T_{NAT} were taken from Hanson and Mauersberger (1988). The absolute values obtained for

T_{NAT} are typically about 198 K. In the vertical regions where enhanced continuum absorption indicates the presence of PSCs temperatures below T_{NAT} are found. The only exceptions are the two spots situated around 17.5 km in section C with the retrieved temperatures slightly above calculated T_{NAT} (i.e. less than 1 K), which are probably due to the limited vertical resolution of MIPAS-STR, uncertainties of the involved retrieval results and effects from horizontal gradients along the viewing direction. For example, the PSC layer might be located in a colder region along viewing direction, while warmer temperatures in other sections along viewing direction might lead to a warmer net temperature retrieved. Furthermore, the values obtained for T_{NAT} are sensitive to potential local variations in the mixing ratios of H_2O (compare Khaykin et al., 2013) and retrieved HNO_3. The sensitivity of calculated T_{NAT} towards variations in the mixing ratios of these gases is shown in Figure 6 and can serve as an estimate for the impact of horizontal gradients.

In Figure 5, the associated vertical distribution of HNO_3 along flight track retrieved from the MIPAS-STR measurements is shown. Local maxima of HNO_3 are found at altitudes ranging from 15.5 to 17.0 km. In sections A and B maximum volume mixing ratios of HNO_3 of 8.5 ppbv are found compared minimum values below 6.5 ppbv around. The maxima in section B_1 to B_3 peak at about 10 ppbv above flight altitude and 11 ppbv at 16.5 km compared to minimum values around 7 ppbv in between. Another strong maximum is observed in section C peaking at 15.5 to 16 km altitude and shows enhanced HNO_3 mixing ratios of 10.5 ppbv compared to minimum values of less than 6 ppbv around. This indicates an excess of HNO_3 resulting from nitrification, with denitrified airmasses above. The resolved vertical thickness of the local HNO_3 maxima is in the order of 1 km. The locations of the HNO_3 maxima show considerable coincidence with the regions where the retrieved temperatures approach T_{NAT}.

Typical profiles retrieved from the MIPAS-STR observations, estimated uncertainties and vertical resolutions are shown in Figure 6. For the temperature retrieval (Fig. 6a), typical vertical resolutions in of 2 to 3 km were obtained, while the estimated 1σ-uncertainties are typically 0.7 to 0.8 K (slightly higher vertical resolutions were obtained in the other flight sections). For continuum absorption two distinct maxima are found peaking at 17.5 and 19 km, indicating two

different PSC layers. The typical vertical resolution obtained is about $1\,\mathrm{km}$. It is pointed out that the alignment of the PSC layers in the horizontal direction along the line-of-sight is uncertain.

Also shown is the corresponding profile of calculated T_{NAT} considering the nominal values for HNO_3 (MIPAS-STR) and H_2O (FLASH-A smoothed) together with the same profiles considering biases of +10% for the volume mixing ratios of these gases. The retrieved temperature is equal to T_{NAT} at about $16\,\mathrm{km}$ altitude and supersaturated conditions are found above. The continuum absorption maximum associated to the lower PSC layer peaks $1.5\,\mathrm{km}$ above, indicating that supersaturated conditions are also present at regions with weak continuum absorption (i.e. cloud-free). The retrieved temperatures above $16\,\mathrm{km}$ are below T_{NAT} by up to about $2.5\,\mathrm{K}$. The shifts in T_{NAT} due to enhanced HNO_3 and H_2O are comparable to or below the uncertainties of the retrieved temperatures.

Figure 6b shows the retrieved profiles of HNO_3 with typical 1σ-uncertainties of 10 % and a high vertical resolution of about $1\,\mathrm{km}$ above $15\,\mathrm{km}$ altitude. The corresponding HNO_3 profile from the CLaMS standard scenario is shown for comparison together with simulated passive NO_y^* (i.e. considering no condensation and vertical redistribution of HNO_3). The comparison shows that the maxima observed by MIPAS-STR peaking at about 16 and $18\,\mathrm{km}$ are reproduced well, reminding that vertical fine structures in the order of $1\,\mathrm{km}$ and localised profiles are considered. The simulated peak values are each by about $2\,\mathrm{ppbv}$ higher than the retrieved values and the lower maximum is significantly shifted towards lower altitudes by 0.5 to $1.0\,\mathrm{km}$. Considerably higher simulated HNO_3 mixing ratios compared to the observation are found above $18\,\mathrm{km}$. While even fine structures are reproduced well by the simulation, the observed discrepancies of the individual profiles are primarily attributed to the complex PSC scenery observed. Based on the assumption that the observed HNO_3 maxima had just evolved or were still developing, the results shown in Figures 5 and 6 strongly support denitrification by particles composed of NAT.

So in summary, (i) the in situ observations of large potential NAT particles, (ii) the retrieved vertical cross-section of continuum absorption indicating extended PSC coverage along flight track and (iii) the observed HNO_3 maxima vertically coinciding with the temperature levels equal to T_{NAT} suggest an ongoing denitrification process with NAT particles being involved.

Interestingly, the retrieved continuum distribution shows no significant continuum enhancement within typically $1.0\,\text{km}$ to $1.5\,\text{km}$ above the levels characterised by temperatures equal to T_{NAT} and where the HNO_3 maxima are found.

Considering the in situ observations of large potential NAT particles with sizes of tens of µm (Fig. 1) at the lower edge of the PSC (Fig. 4, section B) and potentially capable of settling several hundreds of meters per day (compare Pruppacher and Klett, 1997; Fahey et al., 2001), the shown scenario would be compatible with very few large NAT particles falling out of a dense PSC around flight altitude and above (e.g. mixed phase PSC containing STS and NAT) and evaporating at altitudes with temperatures above T_{NAT}. This is furthermore supported by the fact that the FSSP-100 started detecting potential NAT particles already around $17\,\text{km}$ altitude during the ascent phase and below the PSC detected by MIPAS-STR in this region (compare Fig. 4, sections A and B).

5 CLaMS simulations and comparison with MIPAS-STR

The analysis described in the following investigates the impact of reduced settling velocities of NAT particles on the denitrification process. Reduced settling velocities are expected for (i) approximately spherical NAT particles with low mass density and (ii) aspheric NAT particles, which might explain the in situ observations of large particles on 25 January 2010. For this purpose, different CLaMS scenarios considering particle settling velocities reduced by constant factors were carried out, and the impact on the fingerprint in the simulated vertical redistribution of HNO_3 was analysed. The different CLaMS scenarios discussed in the following are summarized in Table 1.

In the following, MIPAS-STR measurements of vertical redistribution of HNO_3 through denitrification are compared with the results from the different CLaMS scenarios for the two vortex flights on 25 January 2010 and 30 January 2010. As discussed above, the first flight was carried under the conditions of synoptic scale PSCs and probably ongoing denitrification and nitrification. The second flight was performed on 30 January 2010 under conditions free of PSCs. The tangent points of the MIPAS-STR observations during this flight (not shown) with start

and landing in Kiruna were located between 63 to 71° N and 1° W to 11° E. The MIPAS-STR measurements between 07:30 and 09:00 UTC were all situated well within the vortex according to the definition of Nash et al. (1996) at the potential temperature level of about 430 K as determined from the ECMWF ERA-Interim reanalysis. The cloud index values of the MIPAS-STR observations associated to this flight indicated cloud-free conditions at stratospheric altitudes (i.e. values higher than 4 according to Spang et al., 2004) and the retrieved temperatures were above calculated T_{NAT}.

As the horizontal resolution along viewing direction and the vertical resolution of the MIPAS-STR observations is somewhat lower compared to the CLaMS simulations, local atmospheric structures are resolved less sharply. Therefore, to consider for effects from atmospheric inhomogeneities in horizontal direction, the CLaMS results were extracted (i) directly at the individual virtual tangent points (i.e. spatial interpolation of the finer retrieval grid onto the tangent point geolocations) of the MIPAS-STR measurements and also the same positions shifted (ii) towards and (iii) away from the observer by the half-distance between observer and nominal virtual tangent point, weighted with a ratio of $3 : 1 : 1$. Measurements at and above flight altitude were also smoothed horizontally in a similar manner by extracting the model results at the observer coordinates and two further positions along the viewing direction. This simple approach allows for a useful approximation of the limited horizontal resolution of an infrared limb-sounder along viewing direction, which typically increases from several tens to a few hundreds of kilometres from the observer altitude towards lower altitudes (compare Ungermann et al., 2012). Furthermore, the vertical smoothing inherent to the MIPAS-STR measurements was taken into account by smoothing the resulting CLaMS profiles with the averaging kernels of the corresponding retrieved MIPAS-STR profiles according to Rodgers (2000).

Figure 7 shows the vertical cross-section of HNO_3 obtained from the CLaMS standard scenario $v = 100\%$ ("v" stands for relative settling velocity, compare Table 1) corresponding to the result from MIPAS-STR shown in Figure 5. A considerable degree of agreement is found between the presented MIPAS-STR and CLaMS results, reminding that narrow vertical and horizontal structures are considered, approaching the resolution of the background fields from ECMWF used for the simulations. The weak local HNO_3 maxima indicated by the MIPAS-STR

14

result in sections A and B around 16 km altitude are faintly reproduced by CLaMS between 06:15 and 06:45 UTC, while CLaMS produces higher HNO_3 mixing ratios and additional local maxima above. The HNO_3 enhancement found in the MIPAS-STR results for the scans B_1 to B_3 around and above flight altitude is also reproduced well, while the maximum around 16 km is only weakly identified in the simulation. In the last section, the strong HNO_3 maximum located at 15.5 to 16.0 km is reproduced well by CLaMS, while another weaker maximum centered at 17.5 km found in the CLaMS result is not identified in the MIPAS-STR cross-section (the vertically constant HNO_3 enhancement above 16 km in the CLaMS cross-section in the first scan of section C are an artefact from the smoothing procedure).

From this comparison it can be seen that mesoscale structures found in the MIPAS-STR results are reproduced by CLaMS in a similar manner. While quality of the agreement between the MIPAS-STR observations and CLaMS simulations varies for individual profiles and subsections, the corresponding ensemble profiles for entire flights cover significant parts of the polar vortex allow for more meaningful comparisons.

In Figure 8a–d the comparison of retrieved and simulated gas-phase HNO_3 for the flight on 25 January 2010 under PSC conditions is shown. The comparison is performed on levels of constant potential temperature to avoid biases from different pressure and temperature layering in the model domain compared to the atmosphere as seen by MIPAS-STR. All MIPAS-STR datapoints and associated CLaMS datapoints for this flight are plotted where both retrieved temperature and HNO_3 from MIPAS-STR are available. In the case of MIPAS-STR the potential temperature levels were calculated considering retrieved temperatures in combination with the corresponding pressure profiles extracted from ECMWF and used for the retrievals. Comparisons are shown for four different CLaMS scenarios (compare Table 1), including the CLaMS standard setup (settling velocities of simulated NAT particles not modified, $v = 100\%$) and three alternative setups with the simulated settling velocities of NAT particles in the model domain multiplied by constant factors of 0.7 ($v = 70\%$), 0.5 ($v = 50\%$) and 0.3 ($v = 30\%$). Each plot shows (i) retrieved gas-phase HNO_3 from MIPAS-STR, (ii) simulated gas-phase HNO_3 from CLaMS associated to the geolocations of the MIPAS-STR datapoints and (iii) simulated passively transported NO_y^* (without consideration of HNO_3 condensation and vertical redistri-

bution by NAT particle sedimentation) extracted from CLaMS for the same geolocations. The datapoints for NO_y^* from CLaMS were smoothed horizontally and vertically in the same way as for HNO_3. Simulated NO_y^* can be compared directly to simulated and measured gas-phase HNO_3 for the discussed flights, as HNO_3 dominates the NO_y budget in the lower stratosphere under Arctic winter conditions (compare Wiegele et al., 2009).

The comparison of measured and simulated gas-phase HNO_3 relative to NO_y^* shows for all scenarios reduced HNO_3 mixing ratios at potential temperature levels higher than about $420\,K$ (about $17.0\,km$ altitude) and excess HNO_3 at lower altitudes. Reduced HNO_3 mixing ratios above the $420\,K$ level in the model domain are the consequence of HNO_3 being partially condensed in PSC particles and sedimentation of NAT particles, while the excess in HNO_3 at lower levels results from evaporation of settled NAT particles. Accordingly, the simulation confirms that the MIPAS-STR measurements associated to the flight on 25 January 2010 show vertical redistribution of HNO_3 through denitrification and associated nitrification. While the overall scattering of the MIPAS-STR data points is mostly higher than for the simulation and the simulated nitrification maxima are by trend located at slightly lower potential temperature levels (typically by $10\,K$ to $20\,K$), the amplitudes of the de- and nitrification structures show considerable agreement with the measurements for the scenarios $v = 100\,\%$, $v = 70\,\%$ and $v = 50\,\%$ (Fig. 8a–c). In contrast, the scenario $v = 30\,\%$ shows only a weak nitrification signal (Fig. 8d).

Figure 9a–d shows the results of the comparison for the flight on 30 January 2010 under conditions free of PSCs and all previously condensed HNO_3 being released back to the gas-phase. Both the MIPAS-STR and the CLaMS results show a strong maximum peaking at a potential temperature level of $400\,K$. The comparison with simulated NO_y^* also here allows clear assignment to a nitrification structure, while the data points in the upper section above the $420\,K$ level indicate effectively denitrified air. The standard CLaMS scenario with $v = 100\,\%$ (Fig. 9a) reproduces the shape and the range of the HNO_3 mixing ratios derived from MIPAS-STR to a high degree. However, the maximum values are overestimated by about $4\,ppbv$ around the level of $400\,K$, and the maximum of the nitrification pattern is shifted towards lower altitudes compared to the MIPAS-STR result. The scenario $v = 70\,\%$ (Fig. 9b) shows improved agree-

ment with MIPAS-STR, with the maximum values being less overestimated compared to the previous scenario. Furthermore, the overall envelope of the pattern appears more diffuse similar to the MIPAS-STR result. The scenario $v = 50\%$ (Fig. 9c) also shows a high degree of agreement with the MIPAS-STR result. However the envelope of the maximum is shifted towards higher levels of potential temperature, and several datapoints associated to the simulation overestimate the range of the HNO_3 mixing ratios obtained from MIPAS-STR above 420 K. Furthermore, the net denitrification above the level of 430 K is reproduced to a lower degree by the simulation. Finally, in the scenario $v = 30\%$ (Fig. 9d) several datapoints strongly overestimate the maximum mixing ratios obtained from MIPAS-STR above the potential temperature level of 410 K, and the net denitrificiation above the level of 430 K is hardly reproduced.

So in summary, the scenarios $v = 100\%$, $v = 70\%$ and $v = 50\%$ reproduce the de- and renitrification patterns indicated by the measurements to a high degree, while the agreement by trend is best for the $v = 70\%$ scenario. In contrast, the scenario $v = 30\%$ shows only a weak nitrification signal for the flight on 25 January 2010 and significantly underestimates the extent of de- and nitrificiation observed on 30 January 2010 as a consequence of strongly reduced settling velocities of simulated NAT particles.

In the following it is discussed which types of particles are expected to approximately show the settling behaviour simulated in the different CLaMS scenarios. On the one hand, approximately spherical particles with a net mass density lower than $1.62\,\mathrm{g\,cm^{-3}}$ would have lower settling speeds compared to compact spherical particles of the same mass which are usually assumed. On the other hand, compact (i.e. mass density of $1.62\,\mathrm{g\,cm^{-3}}$) needle- or disk-shaped particles would also have reduced settling velocities compared to mass-equivalent compact spherical particles. While of course further more complex combinations of particle shape and density are thinkable and likely, the discussion here will be limited to the discussed test cases.

The first row of column 3 in Table 1 contains the mass density and dimensions of a typical compact spherical NAT particle capable of denitrification as simulated by CLaMS. The diameter of 10 μm approximately corresponds to the sizes of the largest particles found in the CLaMS domain for the flight on 25 January 2010 under the conditions discussed in Sect. 3. Below, the sizes of potential spherical particles with reduced mass density having the same mass and ap-

proximately meeting the relative settling speed condition indicated in column 2 are listed. It is pointed that in all modified CLaMS scenarios the respective settling velocities of the simulated particles were multiplied by constant factors to approximate the settling speeds of alternative particle types. The Cunningham slip correction factors taken into account however were in all cases calculated corresponding to compact spherical particles. When calculating the sizes of mass equivalent alternative particle types approximately meeting the indicated relative settling velocity conditions indicated in column 2 only the mass equivalence and the Stokes equation were considered. Contributions from different Cunningham corrections applying to larger diameters or different sizes as a consequence of reduced particle mass density or to alternative particle shapes were not considered for conversion. However, the slip correction factor for a hypothetic low mass density spherical particle with a diameter of 20 μm is only by about 5 % lower compared to that of a compact spherical particle with a diameter of 10 μm. Furthermore, when transferring the mass of a compact spherical particle of similar size into a compact moderately aspheric particle, the effective difference in the Cunningham correction is expected to be in the same order. As the aim of this work is only to give typical sizes of certain particle classes approximately fulfilling the indicated relative settling velocity conditions rather than a full quantitative assessment, these simplifications are acceptable here.

According to Table 1, a spherical NAT particle with a diameter of 14 μm and a mass density of $0.56\,\mathrm{g\,cm^{-3}}$ would have a settling velocity of approximately 70 % compared to a mass equivalent compact spherical NAT particle in the reference scenario (density of $1.62\,\mathrm{g\,cm^{-3}}$ and diameter of 10 μm). Similarly, mass equivalent spherical particles with diameters of 20 μm and 33 μm and the indicated mass densities would have relative settling velocities of approximately 50 % and 30 %.

Columns 4 and 5 in Table 1 give the dimensions of potential of columnar needle- and disk-shaped particles containing the same mass as the indicated spherical particles and approximately meeting the indicated relative settling velocity conditions. The aspect ratio is the ratio between height and diameter of a cylinder (i.e. column or disk). For estimating the sizes of the indicated aspheric particle types associated to the relative settling velocity conditions the respective hydrodynamic radii were approximated by the corresponding capacitances according to

18

Westbrook (2008). The relation between particle size and capacitance was taken from Smythe (1962). Furthermore, for the disk-shaped particles the approximation for horizontally oriented disks discussed by Westbrook (2008) (reference therein) was taken into account, as potential disk-shaped NAT particles in the considered size regime might show preferentially horizontal orientations under stratospheric conditions.

According to Table 1, a compact columnar (i.e. needle-shaped) particle with a length of 34 μm and an aspect ratio of 7.6 would have a settling velocity of approximately 70 % compared to a mass equivalent spherical particle in the reference simulation. Relative settling velocities of 50 % and 30 % would apply approximately to columnar particles with lengths of 68 μm and 168 μm characterised by the indicated aspect ratios. Furthermore, compact mass-equivalent disk-shaped particles with diameters of 11 μm, 21 μm and 38 μm and the indicated aspect ratios would have relative settling velocities of about 70 %, 50 % and 30 %. We mention however that the simplification regarding the Cunningham slip correction has to be seen critically for the extreme cases.

For the flight on 25 January 2010, for the largest particles masses equivalent to that of compact spherical particles with diameters of less than 12 μm are expected as a consequence of limited growing time (compare Sect. 3). From the in situ observations shown in Figure 1, maximum particle sizes around 30 μm were obtained for this flight. According to Table 1, (i) spherical particles with a rather low mass density of about $0.04\,\mathrm{g\,cm^{-3}}$ and a relative settling velocity of about 30 %, (ii) compact columnar particles with an aspect ratio of about 7.6 and a relative settling velocity of 70 % and (iii) compact disk-shaped particles with an aspect ratio of 0.01 and a relative settling velocity of 30 % would have maximum dimensions (diameter or height, respectively) similar to the maximum sizes indicated by the in situ particle observations. The considered spherical and disk-shaped particles characterised by relative settling velocities of about 50 % also would have maximum dimensions significantly larger than the corresponding particles in the reference simulation, but do not allow to reproduce the maximum sizes indicated by the in situ observations.

On the other hand, the comparisons between simulated and measured HNO_3 redistribution through denitrification show that the simulation considering relative settling velocities of 70 %

for simulated NAT particles compared to the standard scenario by trend result in the best agreement. In contrast, the simulation considering relative settling velocities of 30 % significantly underestimates the vertical redistribution of HNO_3.

We point out that this study is not suitable to determine the properties of NAT particles quantitatively, as it is not clear (i) how the maximum sizes indicated by the FSSP-100 measurements have to be interpreted in context of significantly aspheric particles and (ii) limitations of the comparison between the MIPAS-STR measurements and the CLaMS simulations affect the discussed results. However, considering the discussed results we speculate that the large particles indicated by the in situ observations during the flight on 25 January 2010 were compact elongated NAT particles capable of fast growth to large maximum sizes and characterised by moderately reduced relative settling velocities (in the order of 70 %) compared to mass-equivalent compact spherical particles.

6 Conclusions

This study investigates denitrification and the impact in the Arctic winter stratosphere at the end of January 2010 based on airborne observations and chemistry transport simulations associated to the RECONCILE campaign. The combination of in situ particle observations by the FSSP-100, remote sensing measurements by MIPAS-STR and simulations by the CLaMS suggests that an ongoing denitrification process with NAT particles being involved was observed during the Geophysica PSC flight on 25 January 2010. The analysis of the formation conditions of extremely large particles detected by the FSSP-100 utilizing CLaMS particle backward trajectories shows that these particles can hardly be explained by compact spherical NAT particles.

Using simulations by the CLaMS and observations of MIPAS-STR we studied the impact of reduced settling velocities of large NAT particles on vertical HNO_3 redistribution. The comparisons between measured and simulated vertical redistribution of HNO_3 good agreement especially when the settling velocities of the simulated NAT particles are reduced by a moderate constant factor of 0.7 for the given CLaMS setup. In contrast, a factor of 0.3 results in a significant underestimation of the vertical HNO_3 redistribution by the simulation. Our work

shows that reduced settling velocities significantly modify the simulated vertical HNO_3 redistribution. This aspect is important especially for simulations of Arctic vortices, where HNO_3 redistribution is often limited to frequent periods under supersaturated conditions.

Considering the limited growing time and the comparisons between observed and simulated gas-phase HNO_3 we speculate that the apparent large NAT particles observed on 25 January 2010 have been compact considerably aspheric (e.g. elongated) NAT particles. Such particles could grow to largest optically apparent sizes in a short time while having slightly reduced settling velocities compatible with the results of our limited case study. Mass equivalent spherical NAT particles with low mass density or compact disk-shaped NAT particles are less likely candidates, as considerably lower settling velocities were expected for the corresponding particles that could explain the maximum sizes observed in situ, resulting in increased discrepancies between simulated and observed HNO_3 redistribution.

We point out that the simulated HNO_3 redistribution also depends critically on other parameters affecting the simulation (e.g. temperature biases, temperature fluctuations that are not considered, alternative nucleation scenarios and uncertainties in the mixing ratios of HNO_3 and H_2O) which are not adressed by this work. The presented case study is not capable of determining the settling velocities or the physical appearance of NAT particles quantitatively. Our results however show that the settling velocity of NAT particles is an important parameter in simulations and offer a consistent explanation for the presented observations.

References

Borrmann, S., Luo, B., and Mishchenko, M.: The application of the T-matrix method to the measurement of aspherical particles with forward scattering optical particle counters, J. Aerosol Sci., 31, 789–799, 2000.

Carslaw, K. S., Kettleborough, J. A., Northway, M. J., Davies, S., Gao, R., Fahey, D. W., Baumgardner, D. G., Chipperfield, M. P., and Kleinböhl, A.: A vortex-scale simulation of the growth and sedimentation of large nitric acid hydrate particles, J. Geophys. Res., 107, 8300, doi:10.1029/2001JD000467, 2002.

de Reus, M., Borrmann, S., Bansemer, A., Heymsfield, A. J., Weigel, R., Schiller, C., Mitev, V., Frey, W., Kunkel, D., Kürten, A., Curtius, J., Sitnikov, N. M., Ulanovsky, A., and Ravegnani, F.: Evidence for ice particles in the tropical stratosphere from in-situ measurements, Atmos. Chem. Phys., 9, 6775–6792, doi:10.5194/acp-9-6775-2009, 2009.

Dörnbrack, A., Pitts, M. C., Poole, L. R., Orsolini, Y. J., Nishii, K., and Nakamura, H.: The 2009–2010 Arctic stratospheric winter – general evolution, mountain waves and predictability of an operational weather forecast model, Atmos. Chem. Phys., 12, 3659–3675, doi:10.5194/acp-12-3659-2012, 2012.

Drdla, K., Turco, R. P., and Elliott, S.: Heterogeneous chemistry on Antarctic polar stratospheric clouds: a microphysical estimate of the extent of chemical processing, J. Geophys. Res., 98, 8965–8981, doi:10.1029/93JD00164, 1993.

Fahey, D. W., Gao, R. S., Carslaw, K. S., Kettleborough, J., Popp, P. J., Northway, M. J., Holecek, J. C., Ciciora, S. C., McLaughlin, R. J., Thompson, T. L., Winkler, R. H., Baumgardner, D. G., Gandrud, B., Wennberg, P. O., Dhaniyala, S., McKinney, K., Peter, T., Salawitch, R. J., Bui, T. P., Elkins, J. W., Webster, C. R., Atlas, E. L., Jost, H., Wilson, J. C., Herman, R. L., Kleinbohl, A., and von Konig, M.: The detection of large HNO_3-containing particles in the winter arctic stratosphere, Science, 291, 1026–1031, 2001.

Grooß, J.-U., Günther, G., Müller, R., Konopka, P., Bausch, S., Schlager, H., Voigt, C., Volk, C.M., and Toon, G. C.: Simulation of denitrification and ozone loss for the Arctic winter 2002/2003, Atmos. Chem. Phys., 5, 1437–1448, doi:10.5194/acp-5-1437-2005, 2005.

Grooß, J.-U., Engel, I., Borrmann, S., Frey, W., Günther, G., Hoyle, C. R., Kivi, R., Luo, B. P., Molleker, S., Peter, T., Pitts, M. C., Schlager, H., Stiller, G., Vömel, H., Walker, K. A., and Müller, R.: Nitric acid trihydrate nucleation and denitrification in the Arctic stratosphere, Atmos. Chem. Phys., 14, 1055–1073, doi:10.5194/acp-14-1055-2014, 2014.

22

Grothe, H., Tizek, H., Waller, D., and Stokes, D. J.: The crystallization kinetics and morphology of nitric acid trihydrate, Phys. Chem. Chem. Phys., 8, 2232–2239, doi:10.1039/B601514J, 2006.

Hanson, D. and Mauersberger, K.: Laboratory studies of the nitric acid trihydrate: implications for the south polar stratosphere, Geophys. Res. Lett., 15, 855–858, doi:10.1029/GL015i008p00855, 1988.

Höpfner, M.: Study on the impact of polar stratospheric clouds on high resolution mid–IR limb emission spectra, J. Quant. Spectrosc. Radiat. Transfer, 83, 93–107, 2004.

Höpfner, M., Blom, C. E., Echle, G., Glatthor, N., Hase, F., and Stiller, G.: Retrieval simulations for MIPAS-STR measurements, Smith, W. L. [Hrsg.] IRS 2000: Current Problems in Atmospheric Radiation; Proc. of the Internat. Radiation Symp., St. Petersburg, Russia, 24–29 July 2000 Hampton, Va.: DEEPAK Publ., 2001.

Hoyle, C. R., Engel, I., Luo, B. P., Pitts, M. C., Poole, L. R., Grooß, J.-U., and Peter, T.: Heterogeneous formation of polar stratospheric clouds – Part 1: Nucleation of nitric acid trihydrate (NAT), Atmos. Chem. Phys., 13, 9577–9595, doi:10.5194/acp-13-9577-2013, 2013.

Libbrecht, K. G.: The physics of snow crystals, Rep. Prog. Phys., 68, 855–895, doi:10.1088/0034-4885/68/4/R03, 2005.

Keyser, L. F. and Leu, M.-T.: Morphology of Nitric Acid and Water Ice Films, Microsc. Res. Tech., 25, 434–438, doi:10.1002/jemt.1070250514, 1993.

Khaykin, S. M., Engel, I., Vömel, H., Formanyuk, I. M., Kivi, R., Korshunov, L. I., Krämer, M., Lykov, A. D., Meier, S., Naebert, T., Pitts, M. C., Santee, M. L., Spelten, N., Wienhold, F. G., Yushkov, V. A., and Peter, T.: Arctic stratospheric dehydration – Part 1: Unprecedented observation of vertical redistribution of water, Atmos. Chem. Phys., 13, 11503–11517, doi:10.5194/acp-13-11503-2013, 2013.

Khosrawi, F., Urban, J., Pitts, M. C., Voelger, P., Achtert, P., Kaphlanov, M., Santee, M. L., Manney, G. L., Murtagh, D., and Fricke, K.-H.: Denitrification and polar stratospheric cloud formation during the Arctic winter 2009/2010, Atmos. Chem. Phys., 11, 8471–8487, doi:10.5194/acp-11-8471-2011, 2011.

Marti, J. J. and Mauersberger, K.: Evidence for nitric acid pentahydrate formed under stratospheric conditions, J. Phys. Chem., 98, 6897–6899, doi:10.1021/j100079a001, 1994.

Molleker, S., Borrmann, S., Schlager, H., Luo, B., Frey, W., Klingebiel, M., Weigel, R., Ebert, M., Mitev, V., Matthey, R., Woiwode, W., Oelhaf, H., Dörnbrack, A., Stratmann, G., Grooß, J.-U., Günther, G., Vogel, B., Müller, R., Krämer, M., Meyer, J., and Cairo, F.: Microphysical properties of synoptic scale polar stratospheric clouds: in situ measurements of unexpectedly large HNO_3 containing particles in

the Arctic vortex, Atmos. Chem. Phys. Discuss., 14, 12071–12120, doi:10.5194/acpd-14-12071-2014, 2014.

Müller, R. and Peter, Th.: The numerical modelling of the sedimentation of polar stratospheric cloud particles, Ber. Bunsen. Phys. Chem., 96, 353–361, 1992.

Nash, E. R., Newman, P. A., Rosenfield, J. E., and Schoeberl, M. R.: An objective determination of the polar vortex using Ertel's potential vorticity, J. Geophys. Res., 101, 9471–9478, 1996.

Peter, T. and Grooß, J.-U.: Polar Stratospheric Clouds and Sulfate Aerosol Particles: Microphysics, Denitrification and Heterogeneous Chemistry, in: Stratospheric Ozone Depletion and Climate Change, edited by: Müller, R., RSC Publishing, UK, 108–144, 2012.

Phillips, C.: A technique for the numerical solution of certain integral equations of the first kind, J. Assoc. Comput. Math., 9, 84–97, 1962.

Piesch, C., Gulde, T., Sartorius, C., Friedl-Vallon, F., Seefeldner, M., Wölfel, M., Blom, C. E., and Fischer, H.: Design of a MIPAS Instrument for High-Altitude Aircraft, Proc. of the 2nd Internat. Airborne Remote Sensing Conference and Exhibition, ERIM, Ann Arbor, MI, Vol. II, 199–208, 24–27 June 1996, San Francisco, 1996.

Pitts, M. C., Poole, L. R., Dörnbrack, A., and Thomason, L. W.: The 2009–2010 Arctic polar stratospheric cloud season: a CALIPSO perspective, Atmos. Chem. Phys., 11, 2161–2177, doi:10.5194/acp-11-2161-2011, 2011.

Pruppacher, H. R. and Klett, J. D.: Microphysics of Clouds and Precipitation, 2nd Edn., Kluwer Academic Publishers, Dordrecht, 1997.

Purser, R. J. and Huang, H.-L.: Estimating effective data density in a satellite retrieval or an objective analysis, J. App. Meteorol., 32, 1092–1107, 1993.

Rodgers, C. D.: Inverse Methods for Atmospheric Sounding: theory and Practice, vol. 2 of Series on Atmospheric, Oceanic and Planetary Physics, edited by: Taylor, F. W., World Scientific, Singapore, 2000.

Smythe, W. R.: Charged right circular cylinder, J. Appl. Phys., 33, 2966–2967, doi:10.1063/1.1722514, 1962.

Solomon, S.: Stratospheric ozone depletion: a review of concepts and history, Rev. Geophys., 37, 275–316, doi:10.1029/1999RG900008, 1999.

Spang, R., Remedios, J. J., and Barkley, M. P.: Colour indices for the detection and differentiation of cloud types in infra-red limb emission spectra, Adv. Space Res., 33, 1041–1047, 2004.

Stiller, G. P., von Clarmann, T., Funke, B., Glatthor, N., Hase, F., Höpfner, M., and Linden, A.: Sensitivity of trace gas abundances retrievals from infrared limb emission spectra to simplifying approx-

imations in radiative transfer modelling, J. Quant. Spectrosc. Ra., 72, 249–280, doi:10.1016/S0022-4073(01)00123-6, 2002.

Tabazadeh, A. and Toon, O. B.: The presence of metastable HNO_3/H_2O solid phases in the stratosphere inferred from ER2 data, J. Geophys. Res., 101, 9071–9078, doi:10.1029/96JD00062, 1996.

Tikhonov, A.: On the Solution of Incorrectly Stated Problems and a Method of Regularisation, Dokl. Acad. Nauk SSSR, 151, 501–504, 1963.

Ungermann, J., Kalicinsky, C., Olschewski, F., Knieling, P., Hoffmann, L., Blank, J., Woiwode, W., Oelhaf, H., Hösen, E., Volk, C. M., Ulanovsky, A., Ravegnani, F., Weigel, K., Stroh, F., and Riese, M.: CRISTA-NF measurements with unprecedented vertical resolution during the RECONCILE aircraft campaign, Atmos. Meas. Tech., 5, 1173–1191, doi:10.5194/amt-5-1173-2012, 2012.

von Hobe, M., Bekki, S., Borrmann, S., Cairo, F., D'Amato, F., Di Donfrancesco, G., Dörnbrack, A., Ebersoldt, A., Ebert, M., Emde, C., Engel, I., Ern, M., Frey, W., Genco, S., Griessbach, S., Grooß, J.-U., Gulde, T., Günther, G., Hösen, E., Hoffmann, L., Homonnai, V., Hoyle, C. R., Isaksen, I. S. A., Jackson, D. R., Jánosi, I. M., Jones, R. L., Kandler, K., Kalicinsky, C., Keil, A., Khaykin, S. M., Khosrawi, F., Kivi, R., Kuttippurath, J., Laube, J. C., Lefèvre, F., Lehmann, R., Ludmann, S., Luo, B. P., Marchand, M., Meyer, J., Mitev, V., Molleker, S., Müller, R., Oelhaf, H., Olschewski, F., Orsolini, Y., Peter, T., Pfeilsticker, K., Piesch, C., Pitts, M. C., Poole, L. R., Pope, F. D., Ravegnani, F., Rex, M., Riese, M., Röckmann, T., Rognerud, B., Roiger, A., Rolf, C., Santee, M. L., Scheibe, M., Schiller, C., Schlager, H., Siciliani de Cumis, M., Sitnikov, N., Søvde, O. A., Spang, R., Spelten, N., Stordal, F., Sumińska-Ebersoldt, O., Ulanovski, A., Ungermann, J., Viciani, S., Volk, C. M., vom Scheidt, M., von der Gathen, P., Walker, K., Wegner, T., Weigel, R., Weinbruch, S., Wetzel, G., Wienhold, F. G., Wohltmann, I., Woiwode, W., Young, I. A. K., Yushkov, V., Zobrist, B., and Stroh, F.: Reconciliation of essential process parameters for an enhanced predictability of Arctic stratospheric ozone loss and its climate interactions (RECONCILE): activities and results, Atmos. Chem. Phys., 13, 9233–9268, doi:10.5194/acp-13-9233-2013, 2013.

Wagner, R., Möhler, O., Saathoff, H., Stetzer, O., and Schurath, U.: Infrared spectrum of nitric acid dihydrate: influence of particle shape, J. Phys. Chem. A, 109, 2572–2581, doi:10.1021/jp044997u, 2005.

Westbrook, C. D.: The fall speeds of sub-100 µm ice crystals, Q. J. Roy. Meteor. Soc., 134, 1243–1251, 2008.

Wiegele, A., Kleinert, A., Oelhaf, H., Ruhnke, R., Wetzel, G., Friedl-Vallon, F., Lengel, A., Maucher, G., Nordmeyer, H., and Fischer, H.: Spatio-temporal variations of NO_y species in the northern latitudes

stratosphere measured with the balloon-borne MIPAS instrument, Atmos. Chem. Phys., 9, 1151–1163, doi:10.5194/acp-9-1151-2009, 2009.

Woiwode, W., Oelhaf, H., Gulde, T., Piesch, C., Maucher, G., Ebersoldt, A., Keim, C., Höpfner, M., Khaykin, S., Ravegnani, F., Ulanovsky, A. E., Volk, C. M., Hösen, E., Dörnbrack, A., Ungermann, J., Kalicinsky, C., and Orphal, J.: MIPAS-STR measurements in the Arctic UTLS in winter/spring 2010: instrument characterization, retrieval and validation, Atmos. Meas. Tech., 5, 1205–1228, doi:10.5194/amt-5-1205-2012, 2012.

Woiwode, W.: Qualification of the airborne FTIR spectrometer MIPAS-STR and study on denitrification and chlorine deactivation in Arctic winter 2009/10, Dissertation, Karlsruhe Institute of Technology, Faculty of Chemistry and Biosciences, Karlsruhe, Germany, 2014.

Worsnop, D. R., Zahniser, M. S., Fox, L. E., and Wofsy, S. C.: Vapor Pressures of Solid Hydrates of Nitric Acid: implications for Polar Stratospheric Clouds, Science, 259, 71–74, 1993.

Table 1. CLaMS scenarios considering reduced settling velocities for simulated NAT particles (v = velocity, D = diameter, ρ = particle mass density, h = height, AR = aspect ratio).

Model setup		Corresponding particle properties		
Scenario	Relative settling speed	Spherical D [μm] / ρ [g cm^{-3}]	Needle-shaped h [μm] / AR	Disk-shaped[a] D [μm] / AR
$v = 100\,\%$	1.00	10 / 1.62	–	–
$v = 70\,\%$	0.7	14 / 0.56	34 / 7.6	11 / 0.44
$v = 50\,\%$	0.5	20 / 0.20	68 / 21.9	21 / 0.07
$v = 30\,\%$	0.3	33 / 0.04	168 / 84.5	38 / 0.01

[a] Assuming horizontally oriented disks (see text).

27
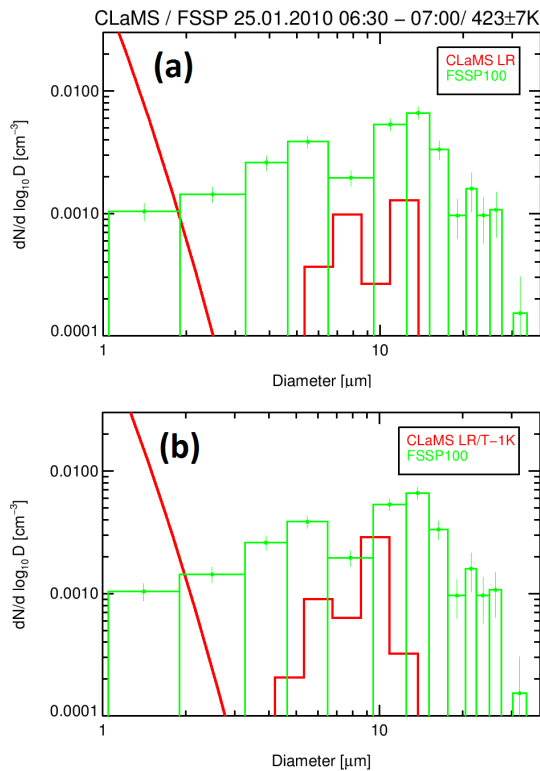
Figure 1. FSSP-100 size distribution (sizes in diameter) derived for the flight on 25 January 2010 for the time interval 06:30 to 07:00 UTC assuming spherical particles (flight altitude 18 km) together with the corresponding size distribution extracted from the CLaMS standard scenario (CLaMS LR). Also shown is the corresponding size distribution considering a temperature bias of -1 K in the simulation (CLaMS LR/T-1K).
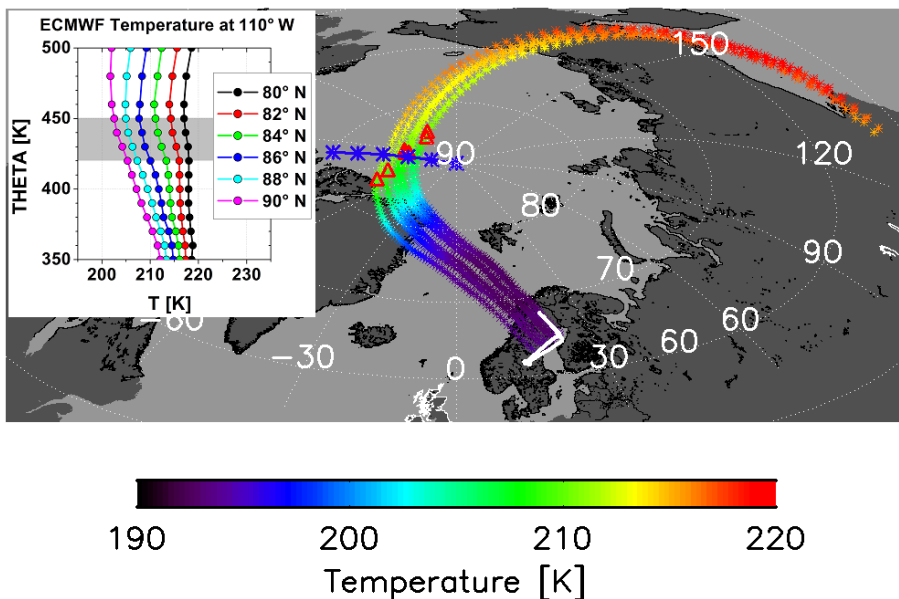
Figure 2. CLaMS sedimentation backward trajectories coloured with temperature (asterisks) for simulated NAT particles with diameters between from 6 to 12 µm associated to the Geophysica flight on 25 January 2010. Prior to the nucleation events the particle trajectories are continued by airmass trajectories for the air volumes where nucleation occurred. The flight track of the Geophysica is indicated by a solid white line. Positions where the trajectories reach 210 K are marked by red triangles. Blue asterisks connected by a blue line indicate the positions of the temperature profiles shown in the inset. The grey shading in the inset indicates the potential temperature (THETA) levels corresponding to the vertical range of about 18 km to 20 km in the model domain (from Woiwode, 2013, with modifications).
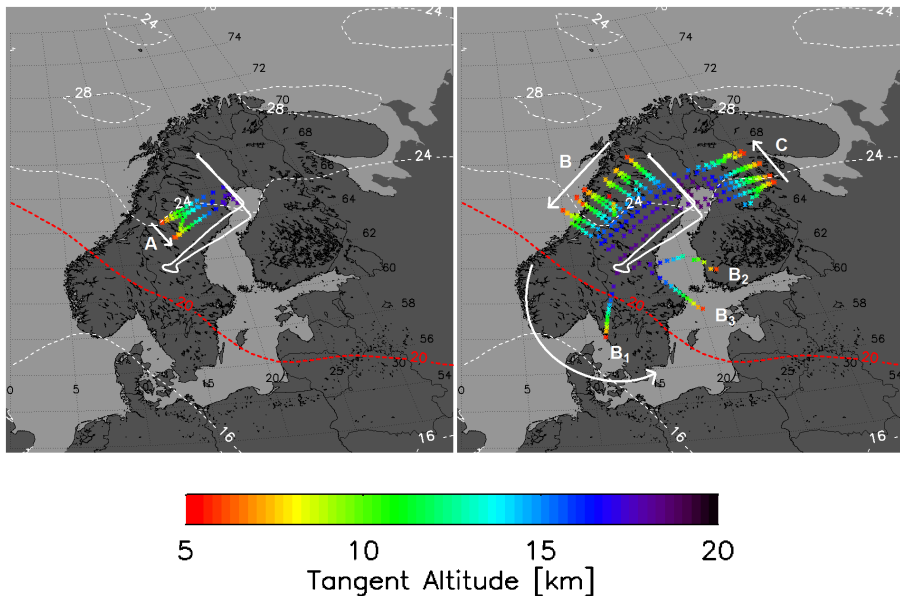
Figure 3. Tangent points associated to the MIPAS-STR measurements during the flight on 25 January 2010 colour-coded with altitude (asterisks). The location of the polar vortex is indicated by isolines of potential vorticity (dotted white lines, values in PVU) at the potential temperature level of 430 K (approximately 18 km) as extracted from the ECMWF ERA-interim reanalysis. The vortex edge is indicated according to Nash et al. (1996) by the red dotted line (from Woiwode, 2013, with modifications).
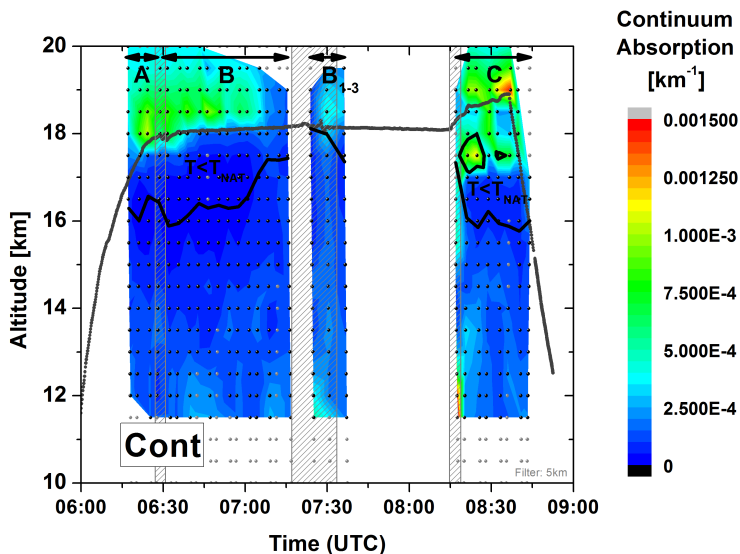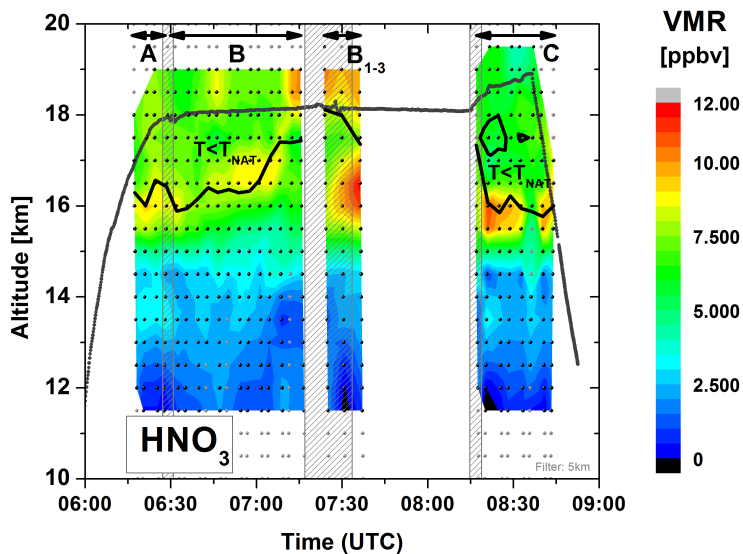
Figure 4. Vertical cross-section of continuum absorption retrieved from the MIPAS-STR observations associated to the flight on 25 January 2010. Enhanced continuum absorption indicates cloud/aerosol particles. The solid black lines indicate levels where temperatures retrieved from MIPAS-STR are equal to calculated T_{NAT} (see text). The flight altitude of the Geophysica is indicated by a solid grey line. The retrieval grid is indicated by black dots. Grey dots were excluded from interpolation due to low vertical resolution. Grey hatched areas indicate turns performed by the Geophysica, where the retrieval results are characterised by increased uncertainties (from Woiwode, 2013, with modifications).

Figure 5. Vertical cross-section of gas-phase HNO$_3$ retrieved from the MIPAS-STR observations associated to the flight on 25 January 2010. Other parameters as in Fig. 4 (from Woiwode, 2013, with modifications).
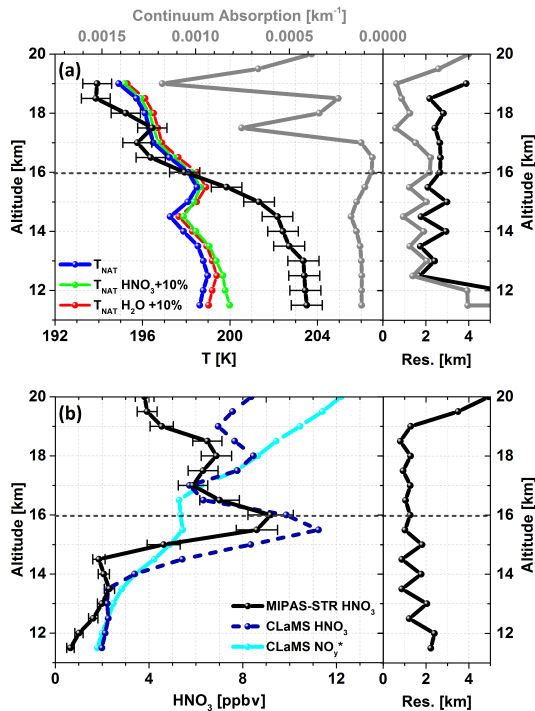
Figure 6. Upper panel (a): Temperature (T) and wave-number independent background continuum absorption (compare Fig. 4) retrieved from MIPAS-STR for the limb scan at 08:32 UTC. Corresponding profiles of T_{NAT} were calculated considering retrieved temperature and HNO_3 in combination with the smoothed H_2O profile from FLASH-A (alternative profiles considering increased HNO_3 and H_2O are also indicated). Lower panel (b): Corresponding profiles of HNO_3 retrieved from MIPAS-STR and extracted from CLaMS together with simulated passive NO_y^*. Res. Corresponds to vertical resolution of the retrieved profiles and error bars to estimated total 1σ-uncertainties of the retrieval results. Grey dotted lines indicate altitude with T equal to T_{NAT}.
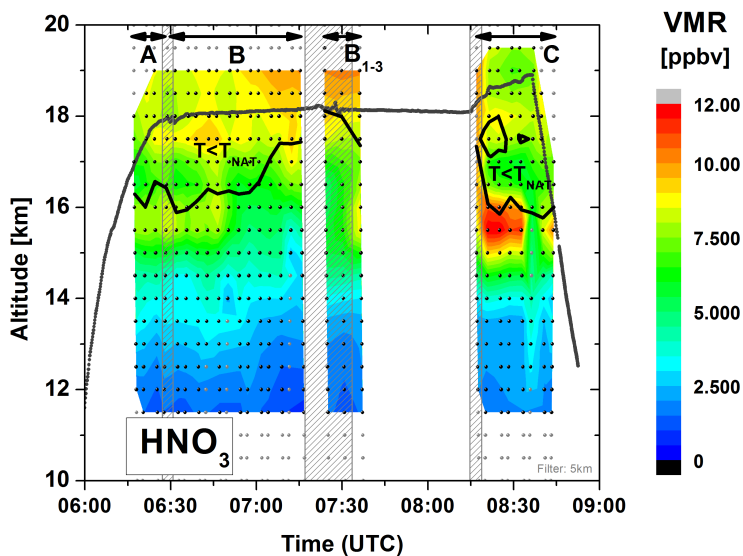
Figure 7. Vertical cross-section of gas-phase HNO_3 extracted from the CLaMS standard scenario $v = 100\%$ (nominal settling velocities) for the flight on 25 January 2010. Other parameters (including T_{NAT}-line) as in Fig. 4.
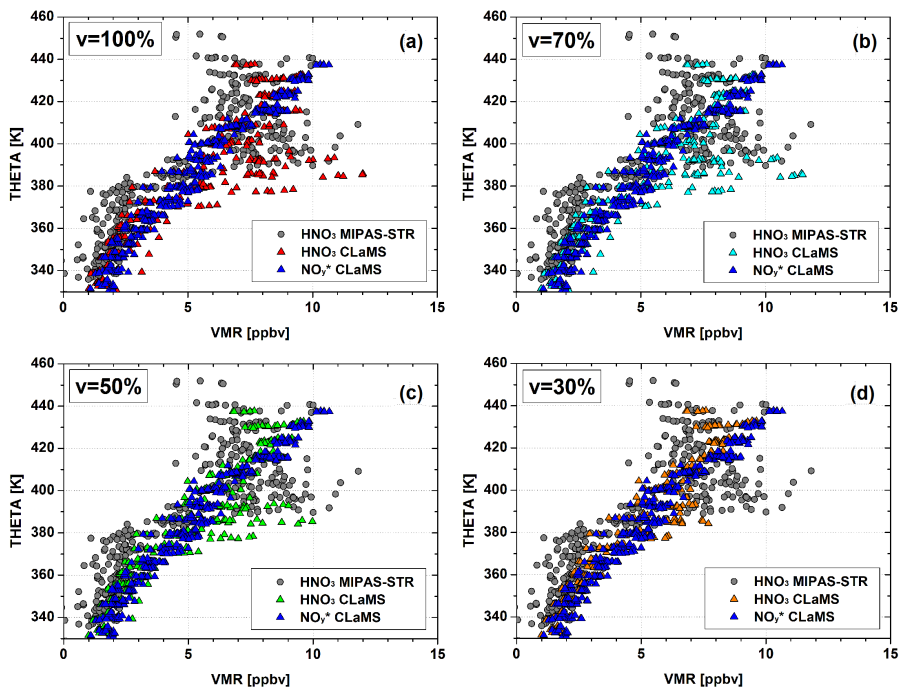
Figure 8. Comparison of measured and modelled vertical distributions of HNO_3 for the flight on 25 January 2010 under PSC-conditions, considering reduced settling velocities for simulated NAT particles. NO_y^* corresponds to simulated passive NO_y.
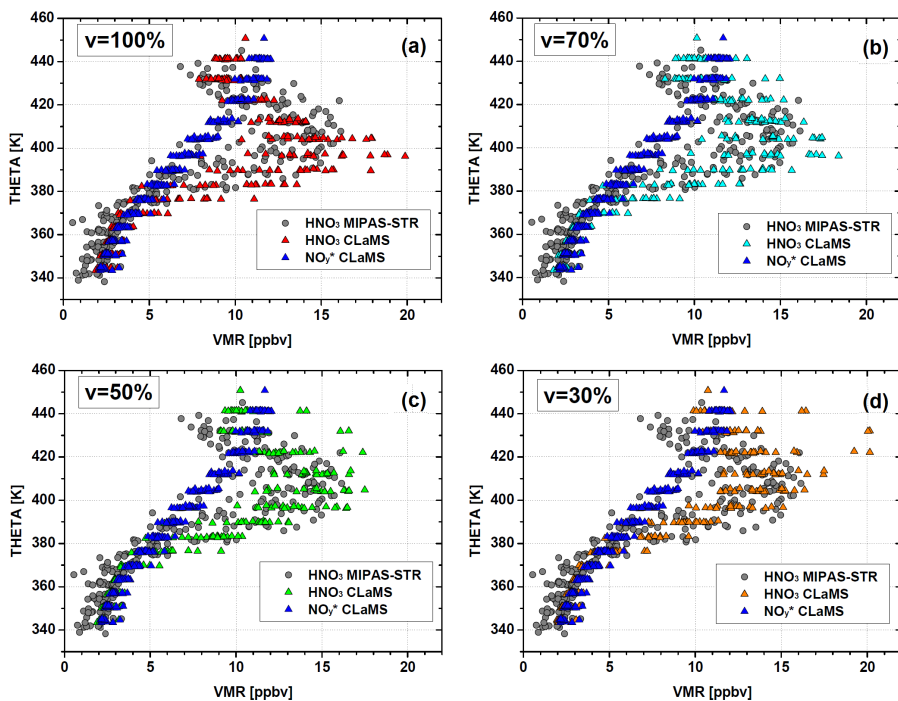
Figure 9. Same comparison as in Fig. 8. for the flight on 30 January 2010 under conditions free of PSCs.